Heliyon 9 (2023) e13023

Contents lists available at ScienceDirect

Heliyon

journal homepage: www.cell.com/heliyon

Research article

Effect of precursor concentration on stoichiometry and optical properties of spray pyrolyzed nanostructured NiO thin films

Victor Adewale Owoeye [a], Saheed Adekunle Adewinbi [b], Ayodeji Olalekan Salau [c,f,*], Ayodele Nicholas Orelusi [a], Abiodun Eyitayo Adeoye [d], Adedeji Tomide Akindadelo [e]

[a] Department of Physical and Chemical Sciences, Elizade University, Ilara-Mokin, Nigeria
[b] Department of Physics, Osun State University, Osogbo, Osun State, Nigeria
[c] Department of Electrical/ Electronics and Computer Engineering, Afe Babalola University, Ado-Ekiti, Nigeria
[d] Department of Physical Sciences, First Technical University, Ibadan, Nigeria
[e] Department of Basic Sciences, Babcock University, Ilishan Remo, Nigeria
[f] Saveetha School of Engineering, Saveetha Institute of Medical and Technical Sciences, India

ARTICLE INFO

Keywords:
Thin films
Precursor
RBS
Opto-electronic
Molarity
Thickness

ABSTRACT

In this study, spray pyrolysis was used to produce nanostructured NiO thin films from high purity nickel acetate ($Ni(CH_3COO)_2.3H_2O$) precursors on pre-heated ultrasonically cleaned soda-lime glass substrates. The metallic constituent concentrations in the films were varied, and the precursors were produced in distilled water at various molarities ranging from 0.1 to 0.4 M. In the study, the field-emission scanning electron microscope (FESEM) results strongly confirmed adherence of the films to the glass substrate at 350 °C. The presence of Ni and O in the samples was confirmed using Rutherford backscattering spectroscopy (RBS), X-ray diffractometry (XRD) and energy dispersive X-ray spectroscopy (EDX). For the 0.1 M NiO thin films, the thickness was approximately 43 nm, and for the 0.2 M, 0.3 M, and 0.4 M films, the thickness was 46 nm, 47 nm, and 49 nm, respectively. The XRD findings were supported by the increased Raman intensity peaks with increased precursor concentration, which confirmed the films' improved crystallinity. For the same number of passes of films deposition, as the molar concentration increases, the films thickness increases. The amount of nickel in NiO thin films increases as the molarity increases, but the amount of oxygen in NiO thin films decreases as the molarity increases. It was discovered that as molarity increases, the optical transmittance decreases and the optical band gap narrows. The qualities of NiO discovered in this study suggest the films' potentials for usage as window layer and buffer material in thin film solar cells.

1. Introduction

Around 13% of the world's population does not have access to reliable energy. Many developing countries are still striving to find electricity that is reliable and inexpensive. Most of the worlds economies are seem to grow once the problem of epileptic power supply is fixed. Solar energy as a renewable energy source has significantly improved the security of electricity. Solar cells or solar panels convert solar energy into electricity, however solar cells are made from components that are both expensive and scarce in nature. It is

* Corresponding author. Department of Electrical/ Electronics and Computer Engineering, Afe Babalola University, Ado-Ekiti, Nigeria.
E-mail address: ayodejisalau98@gmail.com (A.O. Salau).

https://doi.org/10.1016/j.heliyon.2023.e13023
Received 25 September 2022; Received in revised form 12 January 2023; Accepted 13 January 2023
Available online 16 January 2023

therefore important to replace solar cells with organic and inorganic metal oxides with appreciable band gaps.

In recent years, the development of alternative energy sources such as wind, biomass, and solar, among others, has gained traction. One of the key motivations is the rise in environmental concerns relating to the greenhouse potential effects for future generations. In 2013, fossil fuels accounted for nearly 80% of all energy produced, making them the villains responsible for the greenhouse impact. Fortunately, thanks to the utilization of renewable energy sources, this dependence has diminished in recent years [1,2]. Renewable energy, in particular, solar energy has been identified as a critical alternative solution to the current electricity crisis. In recent years, dye-sensitized solar cells (DSSC) have become increasingly important in solar power generation. It was discovered that adding more cells to a cell stack in a Tandem cell with a separate band gap improved DSSC performance [1]. PV solar energy output accounts for only 0.7% of the global renewable energy industry, or 22.1% of the total, with nearly 90% of commercialized solar modules based on high-cost monocrystalline and polycrystalline silicon PV cells. As a result, the low representation of the PV market is due to the high cost of producing solar cells, which is a barrier to the widespread adoption of this energy source [3,4].

Nickel II oxide (NiO) is one of the most researched metal oxides due to its low cost and numerous applications, such as electrode material for Li-ion batteries, light-emitting diodes (LEDs), DSSC, catalyst, transparent conducting oxide, photodetectors, electrochromic, gas sensors, photovoltaic devices, electrochemical super capacitors, heat reflectors, photo-electrochemical cell, solar cells, and many opto-electronic devices [5–10]. Nickel oxide (NiO) is a potential material for p-type transparent conducting oxide films due to its exceptional properties, such as its NaCl-type structure, significant band gap energy ranging from 3.25 to 4 eV, strong crystallinity, high chemical stability, and broad-spectrum range of transparency [9,11–13]. When Ni vacancies and interstitial oxygen are increased in the NiO structure, the resistivity of undoped NiO films can be significantly reduced at ambient temperature [14,15]. To change the energy level state of NiO, band gap energy is important. The development of nickel vacancies and interstitial oxygen atoms in the architectures of NiO thin films was identified as the cause of their low resistivity [16]. The stoichiometric ratio of nickel to oxygen atoms has a significant impact on the behavior of NiO. Due to their nonstoichiometry, nickel oxide films undergo various changes, and these changes in properties have various implications depending on the application [17,18].

Almad et al. [19] studied the impact of precursor solutions on the optical and structural characteristics of pyrolyzed NiO thin films deposited on corning glass substrates. The study's X-ray diffraction results revealed that the cubic, polycrystalline NiO films had a preferential 111-orientation in the growth direction and a random in-plane orientation. The binding energies had shifted, according to the deconvolution of the Ni 2p and O 1s core level X-ray photoelectron spectra of nickel oxides made with various precursors. The sprayed NiO films produced from nickel chloride, nickel acetate, and nickel nitrate had optical band gap energies of 3.2, 3.43, and 3.5 eV respectively. The research by Ukoba et al. [20] examined how different precursor concentrations affected the elemental, morphological, and structural properties of NiO films. They observed an increased surface grains with rising precursor solution concentration. There was also a reduction in oxygen concentration as precursor solution increased. Amorphous structure was discovered in their results at 0.25 M concentration, while polycrystalline with cubic structure was found at higher concentrations. It was discovered that the crystallinity of NiO increased as the concentration of the precursor solution increased. The thickness of the films was reported to increase with concentration, and the film strongly adhered to the glass substrate at 350 °C.

Ukoba et al. [21] investigated the effect of NiO films deposition using the Spray Pyrolysis Technique (SPT) for solar photovoltaic cells as a potential device for solving developing-countries electricity problems. The major precursors for NiO thin films deposition were reported to be nickel chloride, nickel acetate, nickel nitrate, nickel hydroxide, nickel sulfate, and nickel formate. The most commonly used and widely available precursors were reported to be nickel chloride and nickel acetate. Unlike nickel acetate, nickel chloride precursor corroded the deposition equipment (spray gun) because it contains an acid (HCl) as a final product, which corroded the spraying gun. The acid also reduces the durability of the final films. Xuan-Hao et al. [22] prepared compact nickel oxide (NiO) thin films on various substrates using a simple SPT. The optical measurement performed show that the NiO films prepared are p-type transparent semiconductors with a band gap of 3.70 $\pm$ 0.05 eV [21]. Obaida et al. [23] prepared NiO thin films from nickel acetylacetonate through pulsed SPT on glass substrates. The study revealed that at low substrate temperatures and short spray time, the obtained films were observed to be amorphous single crystal structure, whereas the films deposited at higher temperatures and long spray time had a cubic phase single crystal structure. The study observed an increase in lattice parameter and crystallite size with increased deposition temperature and spray time. However, NiO strain was observed to decrease with increased deposition temperature and spray time. The energy band gap was estimated to be 3.52–3.89 eV.

One bottom-up technique for nano-structuring materials is the thin film, which is a layer of materials with a thickness of between one and one hundred nanometers (nm), or less than 1 μm. In materials research, thin films technology is crucial because, at the nanoscale, materials demonstrate uniqueness in all their properties, including electrical, optical, thermal, magnetic, mechanical, and anti-corrosion ones [11,24,25]. SPT has been found to have greater advantages over other deposition processes, including being more cost-effective and consuming less power, than all the different thin films deposition methods [26–28]. The thickness, elemental composition, and stoichiometry of most thin layers can be determined using Rutherford backscattering spectrometry (RBS), a precise, non-destructive analytical technique based on ion beams. It is very helpful for both thin films and bulk materials [29,30].

A review of the literature revealed that there are not many studies on ion beam examination of NiO thin films for opto-electronics applications. Consequently, this study used SPT to prepare different molarities (0.1, 0.2, 0.3 and 0.4 M) of NiO thin films from nickel acetate precursor on a soda-lime glass substrate which it has been preheated and ultrasonically cleaned. The RBS was used to measure the thickness, stoichiometry and elemental profile of the films, while the structural characteristics of the samples were analyzed by X-ray diffractometer (XRD) and Raman microscopy, the morphological properties of the samples were examined by field-emission scanning electron microscope (FESEM) and a UV–visible spectrophotometer were used to evaluate their optical properties. The study provided details on the composition, thickness, morphology, structural and optical characteristics of NiO thin films with higher molarities for their prospective usage as photovoltaic devices.

2. Materials and methods

2.1. Material

The substrate used in this study is a commercially available soda-lime glass substrate with dimensions of 6.8 mm in thickness and 241. 8 mm^2 in cross-section. To lower the contamination to a suitable level, the substrates were ultrasonically cleaned with acetone, methanol, and then distilled water. As a precursor source, nickel acetate, which is soluble in distilled water, was employed to synthesize NiO. The choice of nickel acetate precursor over other NiO precursors has been reported by Ref. [21].

2.2. Thin films preparation

In this study, high purity nickel acetate ($Ni(CH_3COO)_2.4H_2O$) precursor was used to synthesize NiO thin films. The precursors were prepared in distilled water at various molarities (0.1, 0.2, 0.3, and 0.4 M). The amount of nickel acetate ($Ni(CH_3COO)_2.4H_2O$) that was dissolved in a specific volume (10 ml) of distilled water to produce various molarities is given in Eqs. (1)–(1)–(3)(1)–(3).

$$\text{Amount (mol)} = \text{concentration} \times \text{volume } \left(dm^3\right) \tag{1}$$

$$\text{Amount (mol)} = \frac{\text{mass (g)}}{\text{molar mass } \left(\frac{\text{g}}{\text{mol}}\right)} \tag{2}$$

$$\text{Mass (g)} = \text{Amount (mol)} \times \text{Molar mass } \left(\frac{\text{g}}{\text{mol}}\right) \tag{3}$$

Substitute amount of substance in Eq. (1) into Eq. (3)

$$\text{Mass (g)} = \frac{\text{concentration} \times \text{volume } \left(dm^3\right) \times \text{Molar mass}}{1000} \tag{4}$$

The 1000 as a denominator in Eq. (4) is due to the relationship between cm^3 and dm^3 (i.e 1 $dm^3 = 1000\ cm^3$), since the volume of the distilled water was measured in cm^3, it is imperative to convert it to dm^3.

To obtain the mass of nickel acetate to produce 0.1 M in 10 ml of distilled water, the following parameters were required.

molar mass of $Ni(CH_3COO)_2.2H_2O = 248.70$ g/mol

concentration = 0.1 M

volume of distilled water = 10 ml = 10×10^{-3}

The quantity of mass that was measured for 0.1 M $= \frac{0.1 \times 248.70 \times 10}{1000} = 0.25$ g.

where 1 $dm^3 = 1000$.

0.2 M $2 \times 0.75 = 0.5$ g.

0.3 M $3 \times 0.75 = 0.75$ g.

0.4 M $4 \times 0.75 = 1$ g.

To produce 0.1–0.4 M precursor solutions, nickel acetate salts of 0.25 g, 0.5 g, 0.75 g, and 1 g were measured and dissolved in 10 ml of distilled water. The precursor solutions were vigorously shaken and allowed to dissolve for a short period of time before being sprayed over a soda-lime glass substrate that had been heated up and held at an extended pressure (4.2 N/m^2) for 60 s. To produce high-quality films, all deposition parameters were optimized [11,24,25]. Eq. (5) describes the chemical process by which liquid nickel acetate precursor was pyrolyzed at 350 °C to produce NiO.

$$Ni(CH_3COO)_2.2H_20 \xrightarrow{\Delta H, 350\ ^\circ C} NiO + 2CO_2 + 2CH_4 + H_2O \tag{5}$$

2.3. Characterization

RBS was used in this study to evaluate the thin films' thickness, elemental composition, and RBS spectra utilizing a $^4He^+$ incident ion beam, 2.2 MeV energy, exit, and scattering angle of 12°, and 168°, respectively. The backscattered data and elemental profiles were fitted using the SIMNRA software code with a fit precision of 0.01 over a range of 300–1200 fit regions [26–29]. Charges in the range of 1–2 C were also employed, and the energy used (2.2 MeV) was determined to be suitable for the examination of the thin films. The electrons were removed from the accelerated beam of negative ions using a stripper channel located inside the high voltage terminal. As a stripper, either a thin carbon foil (2–5 g/cm^2) or a low-pressure gas in a small channel was employed. However, nitrogen gas is typically employed in the RBS measurements at the Center for Energy Research and Development (CERD) laboratory at Obafemi Awolowo University in Ile-Ife. The probe voltage was adjusted at 17.7 kV, and a pre-accelerating voltage of 6.0 kV was used to obtain the total energy of 2.2 MeV. Because Cornell geometry is a type that is available at CERD, Cornell geometry was employed in this project. 2.2 MeV $^4He^+$ beam analysis was performed on the samples. The information was gathered electronically, and CERD-licensed SIMNRA software was used for the analysis. For the simulation of backscattering or forward scattering spectra for ion beam analysis with MeV ions, SIMNRA is an MS Windows software. The layer thickness and element compositions of different components found in the sample and on different layers were calculated using this simulation.

Powdered X-ray diffractometer (XPERT-PRO diffractometer; Analytical BV, Netherlands) with a 0.02° step size in the range of 2θ

values from 35 to 100° reflection geometry and a CoK α-radiation source (λ = 0.178901 nm) at 50 kV and 30 mA was used to analyze the samples' microstructural characteristics. The Witec alpha 300 RAS + confocal micro-Raman microscope (Focus Innovations, Germany) was used to obtain the Raman spectra data at a laser wavelength of 532 nm, 5 mW power, and 120 s acquisition time. The morphology of the samples were examined using a JEOL JSM-7600F Field-Emission Scanning Electron Microscope (FESEM) at the Rolab Research Laboratory of the International Institute of Tropical Agriculture (IITA), in Ibadan, Nigeria. The apparatus has upper and lower secondary electron detectors, a retractable lens backscatter detector, and a high stable probe current. Energy dispersive X-ray spectroscopy (EDX) connected to the FESEM microscope was used to analyze the films' composition and identify the various peaks. The optical characteristics of the produced samples were evaluated using a UV–visible spectrophotometer. However, the RBS analysis of the thickness of the films functioned as a fundamental variable to determine the energy band gap of the films.

3. Results and discussion

3.1. NiO thin films stoichiometry and thickness

Simulated measurements of the films' thickness and composition were performed with the help of the SIMNRA software, and the resulting spectra are presented in Fig. 1. The films are deposited on soda-lime glass substrates as shown in Fig. 1(a–d), with NiO peaks visible as indicated. The substrate is the area that is below the peaks. Table 1 presents the compositions and thicknesses of the films as determined for the NiO films. Since concentration should increase with composition, it is expected that the percent composition of Ni will increase as molarity increases in Table 1. The increase in Ni content as precursor concentration increases may be caused by an increase in surface grains with rising precursor solution concentration [30]. The table makes it clear that as concentration rises, the thickness of the films also rises. From Table 1, it was determined that the films' thicknesses were roughly 43 nm for a 0.1 M NiO and 46 nm, 47 nm, and 49 nm for three other concentrations. It was found that for a given number of films deposition passes, the films' thickness grows as the molar concentration does. The same tendency has been discovered by Refs. [20,31]. In conclusion, NiO thin films' oxygen content decreases with molarity, which is consistent with the findings of [20,32]. The rise in deposition rate, which can also account for the decline in grain orientation and oxygen concentration, was the primary factor in the NiO films' considerable increase in grow rate as molarity increased. NiO's has higher crystalinity with rising precursor solution concentration and may also be

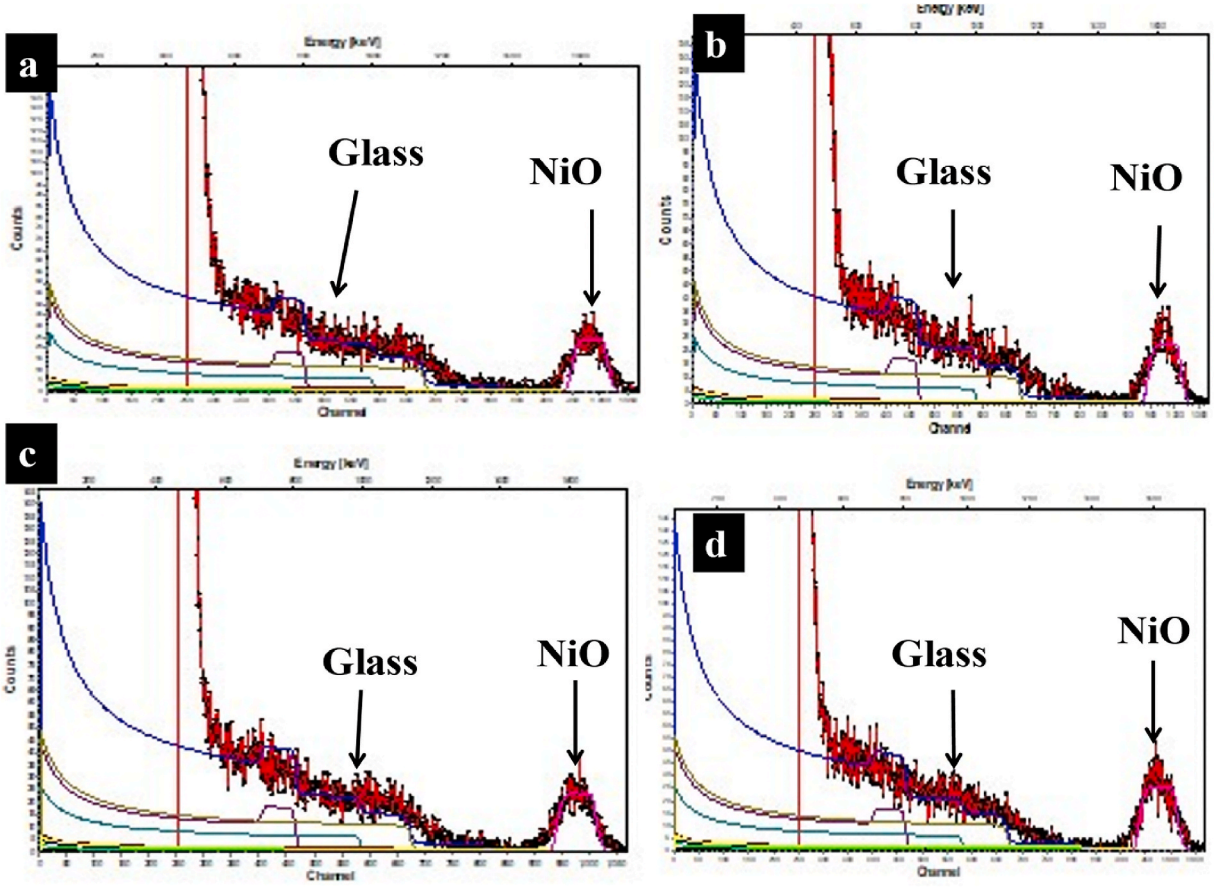

Fig. 1. RBS spectra analysis of NiO thin films (a) 0.1 M (b) 0.2 M (c) 0.3 M (d) 0.4 M.

Table 1
Composition and thickness of NiO thin films.

Thin film	Ni	O	Thickness (nm)
0.1 M	0.09	0.91	43
0.2 M	0.12	0.88	46
0.3 M	0.19	0.81	47
0.4 M	0.24	0.76	49

the cause of the increase in the growth rate of the NiO films as molarity increases.

3.2. NiO thin films' microstructures

Fig. 2 depicts the XRD patterns of (0.1–0.4 M) NiO thin films deposited on soda-lime glass substrates. The figure shows the relationship between intensity (a.u) and position of 2θ (degree). After removing background noise from the diffraction angles, the spectra were displayed within the range of 35°–100°. The results of the SEM micrograph in Fig. 4 and the presence of many diffraction peaks in the XRD spectra both demonstrated that Bragg's law of diffraction had been obeyed and that the deposited films have polycrystalline morphology. The films were found to have five diffraction peaks, with peak (111) being the most prominent, and a single phase NiO cubic crystal structure. The (hkl) indices (111), (200), (220), (311), and (222), which were seen at their respective positions of 2θ, exhibited diffraction peaks that were associated with the cubic NiO crystal structure (COD 96-101-0096; space group Fm-3m) [33]. The NiO phase is stable and forms independently of the substrate temperature as a result of no other peak matching to the other phases in the XRD patterns [34]. The small change in the position of 2θ as the precursor grew is caused by the microstructure of the NiO structure being rearranged because of the higher precursor and deposition temperatures. The small change in the position of 2θ is also as a result of stress or a crystallographic defect in the NiO structure [35]. The Debye Scherrer equation, which is presented in Eq. (6) [36], was used to determine the crystallite size. For thin films produced from NiO containing 0.1–0.4 M, the estimated grain size is 26 nm, respectively. With increased precursor concentration, there was no noticeable change in the grain size. Similar results were reported for 0.025, 0.05, 0.07, and 0.1 M NiO thin films at plane (111) [20]. The XRD result from this study is consistent with the findings of previous studies [20,33,34,36,37].

$$D = \frac{K\lambda}{\beta \cos \theta} \tag{6}$$

where D is crystallite size.

K = Debye constant = 0.90

θ = Diffraction angle

λ = wavelength of the X-ray (λ = 0.178901 nm)

β = FWHM determined for each angle.

The plot of samples' Raman intensity from 1500 to 3000 a.u against wave number from 1000 to 2500 cm^{-1} is shown in Fig. 3. The Raman peaks of (0.1–0.4 M) NiO were formed at the same wave number of approximately 800 cm^{-1}. Raman intensity peaks of 0.1 M and (0.2–0.4) M were measured at 1875, 2250, 2625, and 2995 a.u, respectively. The fact that there was no observable change in the size of the crystallite as the precursor concentration increased could be the cause of the formation of the Raman peaks at the same wavenumber. However, the XRD finding was supported by the increased Raman intensity peaks with increased precursor concentration, which confirmed the films' improved crystallinity. This study's plotted Raman spectra's center Raman peak, which was obtained at 800 cm^{-1} wavenumbers, is consistent with a previous study on the cubic crystal structure of NiO thin films by authors in Ref. [38].

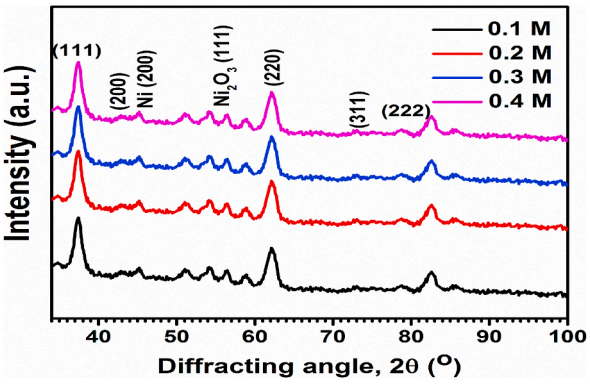

Fig. 2. XRD patterns of NiO thin films.

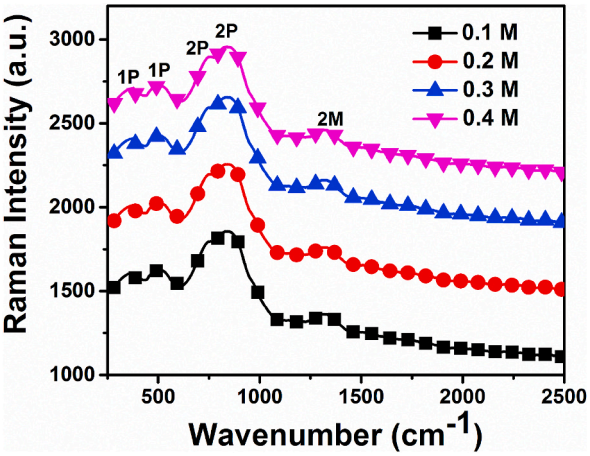

Fig. 3. Raman spectra analysis of NiO thin films.

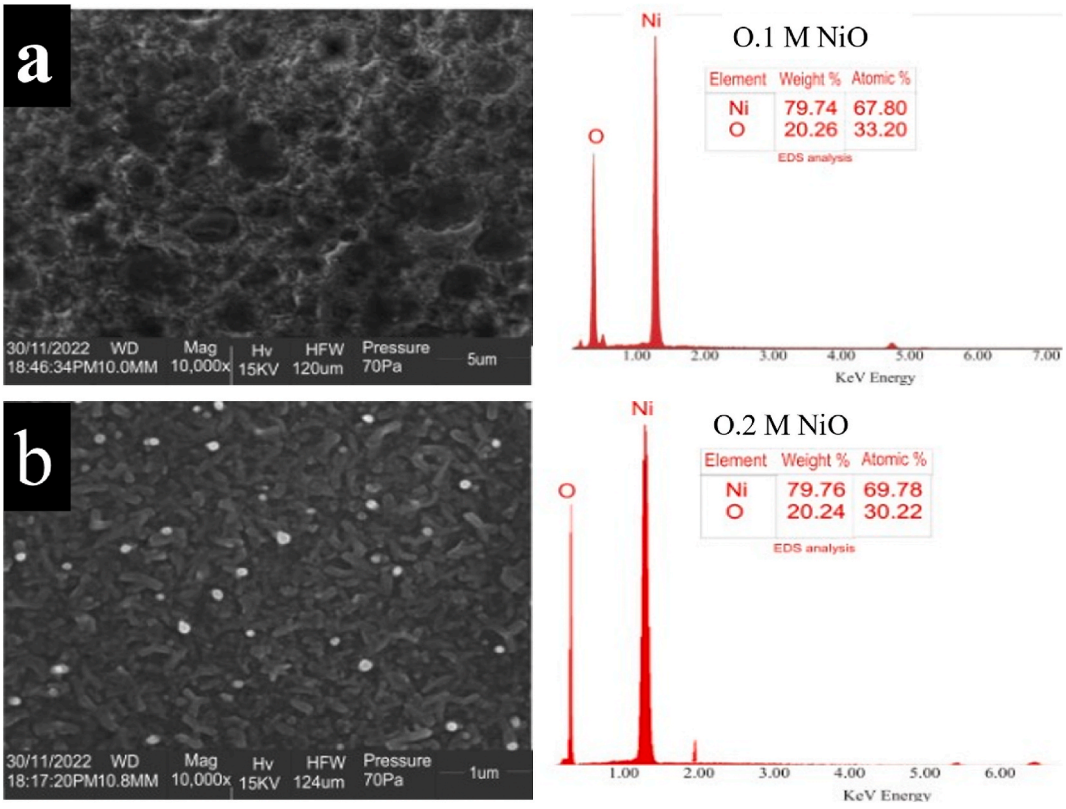

Fig. 4. SEM micrographs and EDX Spectra Analysis of NiO Thin Films (a) 0.1 M (b) 0.2 M.

3.3. Morphological characteristics of the films

The micrographs of 0.1 M and 0.2 M NiO thin films are shown in Fig. 4(a) and (b). There was evidence of surface modification with higher precursor concentration when comparing the micrographs individually. The micrographs showed that the films were evenly spread across the substrate. The FESEM micrographs verified the presence of homogeneous, smooth, well-adhered coatings free of pinholes and cracks as proof of good growth on the substrate surface [20,29]. Strong substrate adherence of thin films in this case, may be caused by the requirement for a pre-heated substrate in the SPT deposition method. The 0.1 M NiO crystal lattice structure shows several visible vacancies in Fig. 4(a). At 0.2 M, it was observed that more NiO grains were occupying the voids, as illustrated in Fig. 4 (b). As seen in Fig. 4(b), there was a clustering of grains that eventually formed a single cubic crystal with a higher precursor

concentration.

The elemental composition of thin films produced from 0.1 to 0.2 M NiO is shown by the EDX spectra in Fig. 4. The findings demonstrate that NiO thin films were successfully deposited on soda-lime glass by the SPT method without impurities because Ni and O were the only elements detected by the EDX probe. In 0.1 M NiO, the percentage composition of the elements was found to be 79.74% Ni and 20.26% O, whereas in 0.2 M, it was found to be 79.76% Ni and 20.24% O. The RBS and XRD results in Figs. 1 and 2, and the EDX result confirmed Ni and O as the primary elemental composition of the deposited films. The EDX results show that the Ni content in NiO thin films increased with precursor concentration, and that the oxygen content decreased with precursor concentration. The increase in films' growth on the glass substrate is the cause of the decrease in oxygen concentration in the deposited NiO films as precursor concentration increased, making less of the glass (oxygen) visible [20].

3.4. Optical properties of the films

The optical properties of spray deposited NiO thin films on glass substrate were examined with the aid of the transmittance and absorbance spectra taking as a function of wavelength (λ) across the ultraviolet (UV)-visible electromagnetic wave spectra ranges (λ: 300–900 nm). The spectra are presented in Figs. 5 and 6. Fig. 5 depicts the transmittance spectra of the prepared films, and the spectra indicate the deposited NiO films exhibit transmittance coefficient falling in the region of 60–80% across the visible range. It can also be observed that the optical transmittance of the spray deposited NiO is dependent on the concentration of the precursor as it declined with increasing precursor. It is expected that when the precursor concentration increased, the films would get thicker, which might ultimately result in a reduction in transmittance since there would be larger clusters and more surface roughness, all of which would enhance light scattering [23]. The increase in NiO molecules with increasing precursor concentration may also cause reduction in the films' transmittance. The incident light will hit several molecules as it travels through the samples, blocking more of it and lowering the transmittance. This feature can be attributed to the increasing surface defects of the films with the precursor concentration which often results into films of higher light attenuation properties [39]. Another contributing factor to the observable trademark in nano-structured spray deposited metal oxide thin films is the thickness of the films which interestingly was found to increase as the molarity of the precursor increases. Increasing thickness of films enhances photon scattering and consequently contribute to free carrier absorption which thus reduces the optical transmission [40,41]. The optical absorption spectra of the deposited NiO thin films samples are depicted in Fig. 6. From the spectra, one could deduce that the films demonstrate low absorption properties in the visible wavelength ranges suggesting the films' potentials for usage as window layer in thin films solar cell [40]. Red shifts can also be observed with respect to increasing precursor concentration. This observable feature found in mesoporous metal oxide nanomaterials have been ascribed to an indication of intrinsic absorption properties attributable to the presence of oxygen vacancy [40,42]. It also suggests the importance of our deposited films as buffer materials capable of being used as charge transport layers for recombination reduction in layered organic solar cell [40]. The optical band gap of the spray deposited NiO thin films are estimated with the use of Tauc's relations in Eqs. (7) and (8).

$$\alpha h\nu = C\left(h\nu - E_g\right)^n \tag{7}$$

$$\alpha = \frac{2.3A}{t} \tag{8}$$

where α is absorption coefficient, h is Planck's constant, ν is the frequency, E_g is the energy band gap, C is constant called band tail parameter, A is absorbance data, while n indicates the optical transition mode which is either 2, 3/2 or ½ for indirect allowed, direct forbidden or direct allowed transitions, respectively [42–44]. Tauc's plots featuring the plots of $(\alpha h\nu)^2$ against $h\nu$ and the extrapolation of the linear path of the plots to the intercepts of the x-axis, were evaluated to exhibit the best fit, thus indicating the deposited NiO thin films demonstrate direct allowed transition property. These plots are presented in Fig. 7 and the estimated values of E_g for each sample are correspondingly indicated on the plots. The variation in the values with the varying precursors' concentration corroborate the

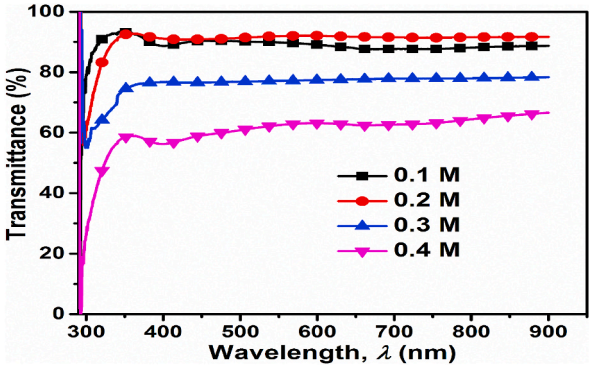

Fig. 5. Optical transmittance spectra analysis of NiO thin films.

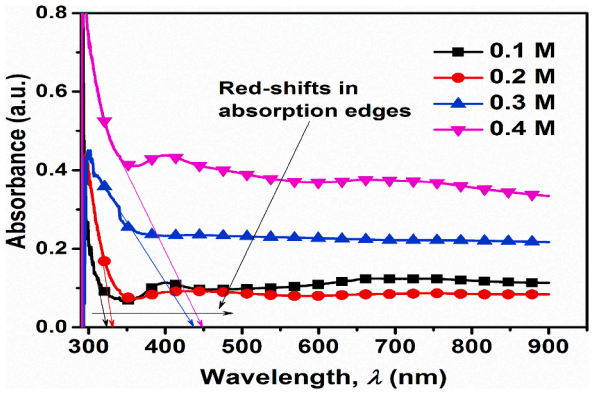

Fig. 6. Optical absorption spectra analysis of NiO thin films.

observable reds shifts of the absorption spectra. The varying bandgap values were also analyzed using Burstein-Moss principle of band shift and the results show the reduction in the band gap energies of the deposited NiO films enhances the material's electrical conductivity by lowering the barrier height for easy hopping of electron [40,42,45].

4. Conclusion

In this paper, an investigation of NiO thin films deposition on soda-lime glass substrate at different precursor concentrations (0.1–0.4 M) from Nickel acetate tetrahydrate precursors using chemical SPT was carried out. The presence of Ni and O in the films was confirmed from the experimental results obtained using the RBS, XRD and EDX. The conclusions drawn from the study's findings are: The concentration increased with composition, as molarity increased, so did the percentage composition of Ni. The oxygen content of NiO thin films was found to decrease with increased molarity. The thickness of the films was obtained as approximately 43 nm for 0.1 M NiO and 46 nm, 47 nm and 49 nm for 0.2 M, 0.3 M and 0.4 M respectively. It was discovered that as the molar concentration increased, so did the films' thickness for the same number of films' deposition passes. The results of the SEM micrograph and the presence of many diffraction peaks in the XRD spectra both show that the deposited films have polycrystalline morphology with single phase cubic crystal structure. Raman intensity peaks increased with precursor concentration, which confirmed the films' improved crystallinity with increased precursor concentration. The optical transmittance of NiO thin films in the UV–visible spectrum (300–900 nm) was found to be highly transparent in the visible spectrum range (60–90%). The optical transmittance of 0.1 M NiO was examined to be approximately 94%, this value decreased to 92, 75 and 62% of 0.2, 0.3, and 0.4 M respectively. The red shifts in absorption edges of NiO were evaluated to be 325, 330, 440 and 450 a.u for 0.1, 0.2, 0.3, and 0.4 M respectively. The band gap value for 0.1 M NiO was estimated to be 4.02 eV, which was observed to reduce to 3. 90, 3.32 and 2.10 eV of 0.2 M, 0.3 M, and 0.4 M respectively. It was discovered that as the molarity of NiO films increased, the optical transmittance decreased, the thickness increased, and optical band gap decreased. The values of the NiO thin films thickness, transmittance and energy bandgap obtained in this study are consistent with those observed in previous studies even at higher molarities. The reduction in the band gap energies of the deposited NiO films enhanced the material's electrical conductivity by lowering the barrier height for easy hopping of electron.

Author contribution statement

Victor Adewale Owoeye: Conceived and designed the experiments; Performed the experiments; Analyzed and interpreted the data; Wrote the paper.

Saheed Adekunle Adewinbi, Abiodun Eyitayo Adeoye: Analyzed and interpreted the data; Contributed reagents, materials, analysis tools or data.

Ayodeji Olalekan Salau: Conceived and designed the experiments; Performed the experiments; Wrote the paper.

Ayodeji Nicholas Orelusi: Contributed reagents, materials, analysis tools or data.

Adedeji Tomide Akindadelo: Conceived and designed the experiments; Analyzed and interpreted the data.

Funding statement

This research did not receive any specific grant from funding agencies in the public, commercial, or not-for-profit sectors.

Data availability statement

Data will be made available on request.

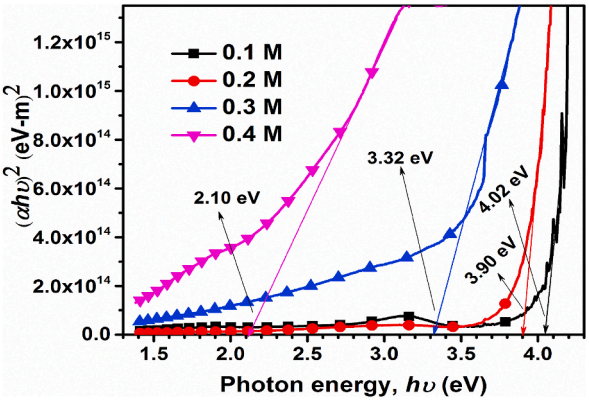

Fig. 7. Optical Band Gap of NiO films.

Declaration of interest's statement

The authors declare no competing interests.

Acknowledgments

The authors gratefully acknowledge the Center for Energy and Research Development at Obafemi Awolowo University in Ile-Ife, Nigeria, for their assistance with this study.

References

[1] A.O. Salau, A.S. Olufemi, G. Oluleye, V.A. Owoeye, I. Ismail, Modelling and performance analysis of dye-sensitized solar cell based on ZnO compact layer and TiO_2 photoanode, J. Mater. Today: Proc. 51 (1) (2022) 502–507, https://doi.org/10.1016/j.matpr.2021.05.592.
[2] A.A. Faremi, A.T. Akindadelo, M.A. Adekoya, A.J. Adebayo, A.O. Salau, S.S. Oluyamo, P.A. Olubambi, Engineering of window layer cadmium sulphide and zinc sulphide thin films for solar cell applications, Results Eng. 16 (2022), 100622, https://doi.org/10.1016/j.rineng.2022.100622.
[3] V. Benda, L. Černá, PV cells and modules – state of the art, limits and trends, Heliyon 6 (12) (2020), https://doi.org/10.1016/j.heliyon.2020.e05666 e05666.
[4] A.A. Amosun, A.O. Salau, O.G. Fadodun, M.A. Jayeola, T.K. Osanyin, M.K. Fasasi, F.I. Ibitoye, Numerical calculation of fuel burn-up rate in a cylindrical nuclear reactor, J. Radioanal. Nucl. Chem. 319 (1) (2019) 459–470, https://doi.org/10.1007/s10967-018-6361-8.
[5] A. Rengaraj, Y. Haldorai, C.H. Kwak, et al., Electrodepositionof flower-like nickel oxide on CVD-grown graphene to develop an electrochemical non-enzymatic biosensor, J. Mater. Chem. B 3 (30) (2015) 6301–6309.
[6] G. Bodurov, T. Ivanova, K. Gesheva, Technology and application of transition metal oxide of WVO as functional layers and NiO thin films as counter electrode material in electrochromic "SmartWindows", Phys. Procedia 46 (2013) 149–158.
[7] Z. He, X. Wang, Renewable energy and fuel production over transition metal oxides: the role of oxygen defects and acidity, Catal. Today 240 (2015) 220–228.
[8] J. Wu, Q. Wang, A. Umar, et al., Highly sensitive p-nitrophenol chemical sensor based on crystalline -MnO2 nanotubes, New J. Chem. 38 (9) (2014) 4420–4426.
[9] R. Sharmaa, A.D. Acharyaa, S.B. Shrivastavaa, T. Shripathi, V. Ganesanb, Preparation and characterization of transparent NiO thin films deposited by spray pyrolysis technique, Optik 125 (2014) 6751–6756.
[10] A.A. Demkov, P. Ponath, K. Fredrickson, et al., Integrated films of transition metal oxides for information technology, Microelectron. Eng. 147 (9913) (2015) 285–289.
[11] V.A. Owoeye, E. Ajenifuja, E.A. Adeoye, G.A. Osinkolu, A.P.I. Popoola, Microstructural and optical properties of Ni-doped ZnO thin films prepared by chemical spray pyrolysis technique, Mater. Res. Express 6 (2019), 086455.
[12] J.C. Osuwa, G.I. Onyejiuwa, Effects of variations in annealing temperature and annealing time on the spectral and solid state properties of nickel oxide (NiO) thin films, Adv. Mater. Res. 787 (2013) 262–268.
[13] X. Chen, Lingzhizhao, and Qiaoliniu, Electrical and optical properties of p-type Li,Cu-codoped NiO thin films, Electron Mater. 41 (2012) 3382–3386.
[14] L. De Los Santos Valladares, A. Ionescu, S. Holmes, et al., Characterization of Ni thin films following thermal oxidation in air, J. Vacuum Sci. Technol. B Nanotechnol. Microelectron. Mater. Proc. Measure. Phenom. 32 (5) (2014) ID051808.
[15] D.S. Kim, H.C. Lee, Nickel vacancy behavior in the electrical conductance of nonstoichiometric nickel oxide film, J. Appl. Phys. 112 (2012) 1–5.
[16] C. Parka, J. Kima, K. Leea, S.k. Oha, H.J. Kanga, N.S. Park, Electronic, optical and electrical properties of nickel oxide thin films grown by RF magnetron sputtering, Appl. Sci. Converg. Technol. 24 (2015) 72–76.
[17] I. Hotovy, L. Spiess, M. Predanocy, V. Rehacek, J. Racko, Sputtered nanocrystalline NiO thin films for very low ethanol detection, Vacuum 107 (2014) 129–131.
[18] H. Moulki, C. Faure, M. Mihelcic, A. Surca Vuk, F. Svegl, B. Orel, G. Campet, A.V. Chadwick, D. Gianolio, A. Rougier, M. Alfredsson, Electrochromic performances of nonstoichiometric NiO thin films, Thin Solid Films 553 (2014) 63–66.
[19] M.M.G. Ahmad, G. Yazdi, S. Schmidt, M. Boshta, V. Khranovskyy, F. Eriksson, B.S. Farag, M.B.S.B. Osman, R. Yakimova, Effect of precursor solutions on the structural and optical properties of sprayed NiO thin films, Mater. Sci. Semicond. Process. 64 (2017) 32–38, https://doi.org/10.1016/j.mssp.2017.03.009.
[20] K.O. Ukoba, A.C. Eloka-Eboka, F.L. Inambao, Influence of concentration on properties of spray deposited nickel oxide films for solar cells, J. Energy Proc. 142 (2017) 236–243.
[21] K.O. Ukoba, A.C. Eloka-Eboka, F.L. Inambao, Review of nanostructured NiO thin film deposition using the spray pyrolysis technique, Renew. Sustain. Energy Rev. 82 (2018) 2900–2915.
[22] C. Xuan-Hao, J.R. Jenning, D. Hossain, K.Z. Yu, Q. Wang, Characteristics of P-NiO Thin films prepared by spray pyrolysis and their application in CdS-senitized photocathodes, Electrochem. Soc. 158 (2011) 733–740.
[23] M. Obaida, A.M. Fathi, I. Moussa, H.H. Afify, Characterization, and electrochromic properties of NiO thin films prepared using a green aqueous solution by pulsed spray pyrolysis technique, J. Mater. Res. 37 (914) (2022) 2282–2292, https://doi.org/10.1557/s43578-022-00627-w.
[24] V.A. Owoeye, E. Ajenifuja, E.A. Adeoye, A.O. Salau, S.A. Adewinbi, A.T. Akindadelo, D.A. Pelemo, A.P.I. Popoola, Effect of precursor concentration on corrosion resistance and microstructure of ZnO thin films using spray pyrolysis method, Scient. African 15 (2022), e01073, https://doi.org/10.1016/j.sciaf.2021.e01073.

[25] V.A. Owoeye, E. Ajenifuja, E.A. Adeoye, A.O. Salau, A.T. Akindadelo, D.A. Pelemo, A.P.I. Popoola, Microstructure and anti-corrosion properties of pray pyrolyzed Ni-doped ZnO thin films for multifunctional surface protection applications, Eng. Res. Expr. 3 (2) (2021), 025012, https://doi.org/10.1088/2631-8695/abf65f.
[26] E. Karakose, H. Çolak, Effect of substrate temperature on the structural properties of ZnO nanorods, Energy 141 (2017) 50–55.
[27] G. Ojeda-Barrero, A.I. Oliva-Avilés, A.I. Oliva, R.D. Maldonado, M. Acosta, G.M. Alonzo-Medina, Effect of the substrate temperature on the physical properties of sprayed-CdS films by using an automatized perfume atomizer, Mater. Sci. Semicond. Process. 79 (2018) 7–13.
[28] M.N. Amroun, M. Khadraoui, Effect of substrate temperature on the properties of SnS_2 thin films, Optik (2019), https://doi.org/10.1016/j.ijleo.2019.03.011.
[29] E. Ajenifuja, G.A. Osinkolu, A.Y. Fasasi, D.A. Pelemo, E.I. Obiajunwa, Rutherford backscattering spectroscopy and structural analysis of DC reactive magnetron sputtered titanium nitride thin films on glass substrates, J. Mater. Sci. Mater. Electron. 27 (2015) 335–341.
[30] G.R. Umapathy, S. Ojha, R. Kavita, M. Thakur, R. Mahajan, N. Kumar, S. Chopra, D. Kanjilal, Composition profile of thin film target by Rutherford backscattering spectrometry, Proc. DAE-BRNS Symp. Nucl. Phys. 61 (2016).
[31] V. Gowthami, M. Meenakshi, Anandhan, C. Sanjeeviraja, Structural and Optical properties of nebulized Nickel Oxide thin films, J. Adv. Microsc. Res. 938 (2014) 103–107.
[32] B.A. Reguig, M. Regragui, M. Morsli, A. Khelil, M. Addou, J.C. Berne′de, Effect of the precursor solution concentration on the NiO thin film properties deposited by spray pyrolysis, J. Solar Energy Mater. Solar Cell 90 (2006) 1381–1392.
[33] M. Wardani, Y. Yulizar, I. Abdullah, D.O.B. Apriandanu, Synthesis of NiO nanoparticles via green route using Ageratum conyzoides L. leaf extract and their catalytic activity, Mater. Sci. Eng. 509 (2019), 012077.
[34] S.A. Mahmoud, S. Alshomer, M.A. Tarawnh, Structural and optical dispersion characterization of sprayed nickel oxide thin films, J. Mod. Phys. 2 (2011) 1178–1186.
[35] V.A. Owoeye, E. Ajenifuja, B. Babatope, G.A. Osinkolu, A.P.I. Popoola, 0. Popoola, Experimental investigation and numerical simulation of mechanical properties and thermal stability of tin alloy processed by equal channel angular extrusion (ECAE), J. Eng. Res. Expr. 1 (2019), 025030.
[36] S.A. Adewinbi, W. Buremo, V.A. Owoeye, Y.A. Ajayeoba, A.O. Salau, H.K. Busari, M.A. Tijani, B.A. Taleatu, Preparation and characterization of TiO_2 thin film electrode for optoelectronic and energy storage potentials: effects of Co incorporation, Chem. Phys. Lett. 779 (2021), 138854, https://doi.org/10.1016/j.cplett.2021.138854.
[37] S.A. Mahmoud, A.A. Akl, H. Kamal, K. Abdel-Hady, Opto-structural, electrical and electrochromic properties of crystalline nickel oxide thin films prepared by spray pyrolysis, Phys. B 311 (2002) 366.
[38] N. Ulmane, A. Kuzmin, I. Sildos, L. Puust, J. Grabis, Magnon and phonon excitations in nanosized NiO, Latv. J. Phys. Tech. Sci. 2 (2019) 61–72.
[39] S. Thota, A. Mallick, S.K. Singh, The role of surface effects on the optical behavior of nanocrystalline NiO, AIP Conf. Proc. 1536 (1) (2013) 521–522 (Vol. 1536, No. 1, pp. 521–522). American Institute of Physics.
[40] S.A. Adewinbi, R.A. Busari, O.E. Adewumi, B.A. Taleatu, Effective photoabsorption of two-way spin-coated metal oxides interfacial layers: surface microstructural and optical studies, Surface. Interfac. 23 (2021), 101029.
[41] K. Anandan, V. Rajendran, Structural, optical and magnetic properties of well-dispersed NiO nanoparticles synthesized by CTAB assisted solvothermal process, Nanosci. Nanotechnol. An Int. J. (NIJ) 2 (4) (2012) 24–29.
[42] S.A. Adewinbi, V.M. Maphiri, B.A. Taleatu, R. Marnadu, M.A. Manthrammel, S. Gedi, Improved photoabsorption and refined electrochemical properties of pseudocapacitive CuxO thin film electrode with Zn incorporation for applications in optoelectronic and charge storage, J. Alloys Compd. 897 (2022), 163151.
[43] C. Mrabet, M.B. Amor, A. Boukhachem, M. Amlouk, T. Manoubi, Physical properties of La-doped NiO sprayed thin films for optoelectronic and sensor applications, Ceram. Int. 42 (5) (2016) 5963–5978.
[44] R. Sharma, A.D. Acharya, S. Moghe, S.B. Shrivastava, M. Gangrade, T. Shripathi, V. Ganesan, Effect of cobalt doping on microstructural and optical properties of nickel oxide thin films, Mater. Sci. Semicond. Process. 23 (2014) 42–49.
[45] E. Burstein, Anomalous optical absorption limit in InSb, Phys. Rev. 93 (3) (1954) 632.